Direct Observation of Solvent-Reaction Intermediate Interactions in Heterogeneously Catalyzed Alcohol Coupling

Eri Muramoto,[‡1] Dipna A. Patel,[‡2] Wei Chen,[‡3,4] Philippe Sautet,[5,6] E. Charles H. Sykes,[2] and Robert J. Madix*[1]

[1]John A. Paulson School of Engineering and Applied Sciences, Harvard University, Cambridge, MA 02138, USA

[2]Department of Chemistry, Tufts University, Medford, MA 02155, USA

[3]Department of Chemistry and Chemical Biology, Harvard University, Cambridge, MA 02138, USA

[4]Center for Functional Nanomaterials, Brookhaven National Laboratory, Upton, NY 11973, USA

[5]Department of Chemical and Biomolecular Engineering, University of California, Los Angeles, CA 90095, USA

[6]Department of Chemistry and Biochemistry, University of California, Los Angeles, CA 90095, USA

ABSTRACT: The relative stability of reactive intermediates and reactants on a surface, which dictates the rate and selectivity of catalytic reactions in both gas and liquid phases, is dependent on numerous factors. One well-established example is secondary interactions, such as van der Waals interactions between the catalyst surface and the pendant group of the intermediate, which can govern reaction selectivity for coupling reactions. Herein, we directly show that interactions between adsorbed reaction intermediates and reactant molecules increase the binding energy and affects the geometrical arrangement of coadsorbed reactant/solvent molecules. Evidence for this effect is demonstrated for the oxidative coupling reaction of methanol on a single crystal gold (Au(110)) surface. The rate-limiting reaction intermediate for methanol self-coupling, methoxy, stabilizes excess adsorbed methanol which desorbs as the result of beta-hydride decomposition of the adsorbed methoxy. Direct molecular-scale imaging by scanning tuneling microscopy, supplemented by density functional theory, revealed interactive structures formed by methoxy and coadsorbed methanol. Interactions between the methoxy intermediate and coadsorbed methanol stabilizes a hydrogen-bonded network comprising methoxy and methanol by a minimum of 0.13 eV per methanol molecule. Inclusion of such interactions between reaction intermediates and coadsorbed reactants and solvents in kinetic models is important to microkinetic analysis of the rates and selectivities of catalytic reactions in both the gas and liquid phases whenever appreciable coverages of species from the ambient phase exist.

INTRODUCTION

Considerable effort has been devoted to understanding the effects of solvation and hydrogen bonding in catalysis,[1] electrochemistry,[2] organic synthesis[3] and surface engineering[4]. For example, it has been shown that the rates of some enzymatic reactions are accelerated by hydrogen bonding, which stabilizes intermediates (thus lowering the activation free energy of their formation) and facilitates proton transfer from an acid or to a base.[5] In heterogeneous catalysis, in both the gas and liquid phases, the interactions of reactive intermediates with a reaction medium can result in alteration of the reaction mechanism and/or the overall kinetics and selectivity.[6–10] For engineering self-assembled monolayers (SAMs), the intermolecular and molecule-substrate interactions of surface-active materials are influenced by solvation, changing their ordering, growth and adhesion.[11–13] Furthermore, solvation of adsorbates on electrodes is known to play a critical role in determining the activity and selectivity of electrocatalytic carbon dioxide reduction reaction (CO_2RR)[14] as well as the capacity and rechargeability of certain batteries.[15,16] Studying the effects of co-adsorbed molecules that may not appear at first glance to take part in a chemical reaction is therefore crucial for understanding the complex interactions that affect the energetics of reactions on surfaces.

Fundamental study of these effects has particular importance in heterogeneous catalysis because the *design* of efficient catalysts requires understanding of all factors that affect the stability of surface species. One important factor is the relative bond strength between different metals and the anchoring atom of reactive intermediates (e.g., C, N, O, S), which can be estimated for transition metal catalysts using scaling relations.[17,18] These bond energies form a basis for the prediction of trends in catalytic activity for different metal catalysts, including binary alloys.[19,20] In addition to these primary interactions, secondary interactions such as van der Waals interactions between pendant groups of intermediates and the catalyst surface have been shown to significantly affect selectivities in catalytic cross-coupling reactions.[21–23] Moreover, inter-adsorbate interactions can induce island formation and surface restructuring, entirely altering the overall kinetics of reaction.[23,24]

Beyond the primary and secondary interactions of reactive intermediates with the surface lies the effects of coadsorbed ***intact*** solvent, reactant or product molecules. There is abundant literature that establishes the importance of hydrogen bonding with water and alcohols on metal and metal oxide surfaces and zeolite cages.[8–10] It has been shown that co-adsorbed molecules may directly participate in reactions, change the stability of reactants, intermediates, transition states and products, and reduce the density of active sites by competitive adsorption with the reactants and intermediates, as discussed in detail in several recent reviews.[8–10] These studies using various catalysts, supports and solvents, combined with theoretical studies, have provided some understanding of solvent effects.[8–10,25–37] However, while numerous scanning tunneling microscopy studies with water have shown hydrogen-bonded water-OH structures that result from dissociation of water on metal oxide[38] and metal[39–44] surfaces as well as hydration of supramolecular assemblies,[12,45,46] direct *in situ* observation of solvent effects for a complex catalytic system is rare, and understanding of the range of molecular ordering induced by such effects is limited.

Given the accepted mechanism for the coupling of alcohols on transition metal catalysts, the possibility of hydrogen bonding between reactants (alcohols), intermediates (alkoxides, aldehydes) and products (aldehydes, esters) can be anticipated and some evidence has been provided by theory,[47–50] but direct experimental demonstration of these interactions for reactive systems has not been made to the best of our knowledge. Indeed, on close-packed Au, Cu and Pt surfaces methanol molecules form well-ordered, hydrogen-bonded networks whose structures depend on the metal as well as the methanol coverage.[51–54] Relatively less is known about adsorption of methanol on the less closely packed surfaces. Furthermore, surface-bound carboxylates form hydrogen-bonded complexes with water and carboxylic acids. For example, on the Ag(110) surface solvation of the transition state by water molecules plays an important role in reducing the kinetic barrier for the formation of the O-bound bidentate species *OCHO, which is a key intermediate in CO_2RR.[55,56] More recently it was suggested with density functional theory (DFT) calculations that hydrogen bonding between formic acid and formate affects the kinetics of formate decomposition on Cu(111).[57,58] Similarly, the interactions between alcohols and surface-bound intermediates may have effects on the thermodynamics and kinetics of alcohol coupling.

The reaction mechanism of oxidative coupling of methanol on gold surfaces has been established previously on both Au(110) and Au(111) surfaces.[59–62] Importantly, knowledge of the elementary reactions provides a quantitative relationship among the amounts of each product formed. The catalytic cycle is initiated by activation of methanol by pre-adsorbed atomic oxygen that selectively cleaves the O–H bond, forming stable methoxy species and water.

$$2CH_3OH + O^* \rightarrow 2CH_3O^* + H_2O^* \quad (1)$$

β-H elimination of methoxy produces surface-bound formaldehyde, which can either couple with unreacted methoxy, desorb or combust via adsorbed formate in the presence of excess surface atomic oxygen.

$$CH_3O^* \rightarrow H_2CO^* + H^* \quad \text{(rate-determining step)} \quad (2)$$

$$H_2CO^* + CH_3O^* \rightarrow H_2COOCH_3^* \quad \text{(coupling)} \quad (3)$$

$$H_2COOCH_3^* \rightarrow HCOOCH_3^* + H^* \quad \text{(ester formation)} \quad (4)$$

$$H_2CO^* + O^* \rightarrow HCOO^* + H^* \quad \text{(over oxidation)} \quad (5)$$

$$HCOO^* \rightarrow CO_2 + H^* \quad \text{(combustion)} \quad (6)$$

The rate-determining step of the coupling reaction, step (2), occurs facilely with an activation energy of energy of 15.4 ± 1.1 kcal[63] (at 225 K in temperature programmed reaction) on Au(110). According to the above reaction scheme, two hydrogen atoms are released in the process of forming one methyl formate molecule (one from methoxy and another from hemi-acetal). These hydrogen atoms may react with methoxy or remaining atomic oxygen to produce methanol or water, respectively, or recombine to form dihydrogen.

$$H^* + CH_3O^* \rightarrow CH_3OH^* \quad (7)$$

$$H^* + \tfrac{1}{2}O^* \rightarrow \tfrac{1}{2}H_2O \quad (8)$$

$$2H^* \rightarrow H_2 \quad (9)$$

In this study the molecule-intermediate-surface (tertiary) interactions that lead to the stabilization of molecular methanol by methoxy were examined by a combination of spectroscopy, microscopy and theory. Temperature programmed spectroscopy was employed to identify reaction intermediates and to separate individual reaction steps by the temperatures at which products were evolved so that they could be separately quantified. Direct imaging of adsorbed methoxy and methanol was performed by scanning tunneling microscopy, while vibrational spectroscopy was used to verify the identity of adsorbed species. Density functional theory was employed to corroborate the differentiation of methanol and methoxy in the microscope images and provided understanding of the spatial organization of the coadsorbed structures. We find that (1) the methoxy reaction intermediate substantially stabilizes molecular methanol on the surface via hydrogen bonding; (2) co-adsorbed methoxy extensively reorients the clusters of adsorbed methanol from their unperturbed structure on the clean surface. More generally, this work directly demonstrates surface interactions between adsorbed reaction intermediates and reactant or solvent molecules that *may* affect the selectivity and kinetics of elementary steps in the catalytic reaction network. Our observations may also be relevant to electrochemical surface scientists interested in the molecular-scale ordering and elementary steps at electrode-electrolyte interfaces.

METHODS SECTION

Temperature-programmed experiments and high-resolution electron energy loss spectroscopy. Temperature-programmed desorption/reaction experiments and vibrational spectroscopy were performed in an ultra-high vacuum (UHV) chamber with a base pressure below 3×10^{-10} Torr, described in detail previously.[21,64] To track the surface reaction the Au(110) single crystal (SPL, 8 mm x 2 mm disk) was radiatively heated using a tungsten filament placed ca. 3 mm behind the crystal. The temperature was monitored by a K-type thermocouple inserted into a pinhole on the side of the crystal. Initial cleaning was performed by repeated cycles of Ar^+ sputtering, annealing and titration by ozone. The surface was cleaned each day with ozone until no CO or CO_2 desorbed during heating after exposure to excess ozone. Temperature-programmed desorption and reaction (TPD/TPR) were performed using a quadrupole mass spectrometer with an ionizer and mass filters contained in a cylindrical shroud (QMS, Hiden HAL/3F). Details about quantitative TPD/TPR analysis can be found in the Supporting Information. High-resolution electron energy loss spectroscopy (HREELS, LK-2000) was performed using a primary energy of 7 eV at 60° specular geometry and obtained spectra were normalized by the average intensity of the flat background region (3650-4000 cm^{-1}).

Methoxy was formed by first exposing the surface to ozone to generate adsorbed atomic oxygen, followed by exposure to methanol (≥99.9% Sigma Aldrich). Gases dissolved in methanol were removed by freeze-pump-thaw cycles. The ozone dosing system consisting of a variable leak valve and stainless-steel tubing was passivated each day by flowing ozone through it for 30 minutes. Ozone was generated by a LG-7 CD Laboratory Ozone Generator and its concentration was monitored by a Teledyne Instruments 454H monitor. Atomic oxygen coverage was calibrated by comparing the integral of the O_2 recombination peak at 560 K to that of the O_2 recombination peak for the saturation coverage of 1 monolayer (ML).[65] Methanol exposures were pre-calibrated separately by condensing methanol on the clean Au(110) surface and performing quantitative analysis of TPD spectra as explained in detail in the Supporting Information.

Scanning Tunneling Microscopy. All STM experiments were performed on an Omicron Nanotechnology low temperature scanning tunneling microscope (LT-STM) under UHV with a base pressure below 5.0×10^{-11} mbar which allowed for 5 K imaging. A Au(110) single crystal (Princeton Scientific) was cleaned via repeated Ar^+ sputtering (1.5 keV, 2 μA) and annealing (750 K) cycles in the preparation chamber with a base pressure < 2.0×10^{-10} mbar. After cleaning, the sample was transferred to the liquid helium (Middlesex Gases) cooled STM stage to image the clean sample at 5 K. After confirming the cleanliness of the single crystal, the sample was warmed to room temperature. Meanwhile, in the preparation chamber, the dosing line was passivated with ozone using a LG-7 CD Laboratory Ozone Generator for 45 minutes. After the line was passivated, the Au(110) sample was transferred into the preparation chamber and exposed to ozone at room temperature to obtain an atomic oxygen coverage of 0.13 ML on the surface. Thereafter the sample was transferred to the STM stage for 5 K imaging.

Methanol (99.8% Sigma Aldrich) was purified using freeze-pump-thaw cycles and 0.5 ML was dosed onto the O pre-covered Au(110) surface at 5 K using a collimated high precision leak valve. Annealing experiments were performed in the STM chamber using the wobblestick and the sample was cooled back down to 5 K before imaging.

Density functional theory calculations. Our DFT calculations were performed with the VASP code.[66] The projector-augmented wave (PAW) potentials[67] and the GGA-PBE exchange-correlation functionals[68] were used. The plane-wave cutoff energy was 400 eV. The DFT-TS method[69] was used to account for the vdW interactions. The lattice constant of Au was obtained via energy optimization. The Au(110) surfaces were represented by slabs of

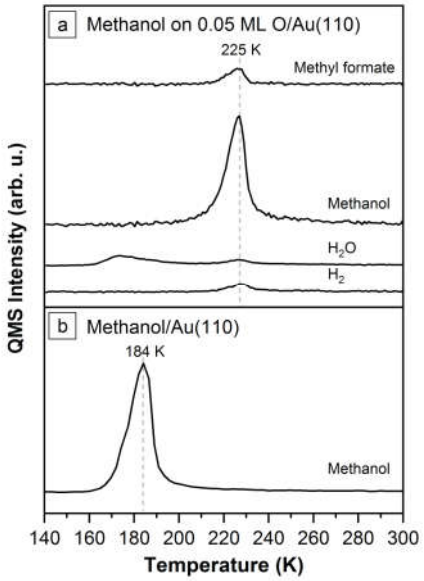

Figure 1. Temperature-programmed reaction/desorption spectra following (a) an exposure of O-covered Au(110) surface to sub-ML methanol and (b) exposure of pristine Au(110) surface to sub-ML methanol, both at 120 K. In the absence of oxygen, methanol desorbed from the surface at T_p=184 K (desorption from multi-layers was observed at 150 K at higher exposures, see Supporting Information). When atomic oxygen was pre-adsorbed, the methanol desorption peak was observed at T_p=225 K, concomitantly with the reaction-limited desorption of methyl formate, molecular hydrogen and water. The desorption of formaldehyde and complete combustion, which occur via formate decomposition at ~300 K, were not observed. QMS signals were corrected to account for fragmentation, differences in transmission and detection coefficients of each fragment and differences in the ionization cross section of molecules[112] as explained in the Supporting Information. Selected fragments: methyl formate (parent m/z=60, fragments m/z=31, m/z=2), methanol (largest fragment m/z=31, fragment m/z=2), water (m/z=18) and dihydrogen (m/z=2). The amount of each detected species is listed in Ta-

five atomic layers. The vacuum region above the topmost atom of the adsorbate was thicker than 14 Å in the z direction, to eliminate coupling between neighboring slabs. During relaxation, Au atoms in the bottom two layers were fixed in their respective bulk positions, and all the other atoms, including the adsorbates, were fully relaxed until the force on each atom was smaller than 0.01 eV/Å. The structures were visualized by VESTA.[70] The STM images were simulated using the electronic states with energies ranging from the Fermi level (EF) to +40 mV. The simulated STM data were then analyzed and visualized by p4vasp. The adsorption energies were calculated using the "separated states" of the relaxed molecules and surface.

To provide reference and energies for evaluating the structures of methoxy and methanol, isolated moieties of O, OH, methoxy, and methanol were first computed (Fig. S5). An exhaustive search including testing of various adsorption sites and orientations of the species was performed. Both O and OH prefer a three-fold hollow site on the side of the topmost row of Au atoms of the Au(110)-(1×2) surface, whereas methoxy prefers a two-fold bridge site and methanol an atop site on the topmost row.

RESULTS

Quantifying desorption of methanol stabilized by methoxy with temperature-programmed reaction spectroscopy. Temperature programmed reaction spectra of oxidative methanol coupling shows that methanol desorbs concomitantly with methyl formate. (Fig. 1). When methanol was dosed to the 0.05 ML O-covered surface at 120 K, evolution of methyl formate, water and dihydrogen was observed at 225 K during heating (Fig. 1a), as expected from previous studies.[59,61,62] Also, as previously reported[59,60,62] a substantial amount of methanol is observed at the same temperature, 40 K above its temperature of desorption from the pristine Au(110) surface (peak temperature T_p of 184 K, Fig. 1b). Previous work on Au(111) and Ag(110) suggest that the origin of this methanol is either the recombination of H atoms released by beta C-H bond cleavage of methoxy with adsorbed methoxy,[60] stabilization by adsorbed oxygen,[60] or stabilization by methoxy.[71] The fact that this feature persists even when there is insignificant amount of coadsorbed oxygen compared to methanol rules out the second possibility in this work. Indeed, quantitative analysis of the desorption peaks (see below) shows that some of this methanol desorbing at 225 K was regenerated from reaction of methoxy with hydrogen atoms released by β-H elimination, but that most is due to intact methanol stabilized by methoxy. This demonstrates that the release of methyl formate from the surface, which occurs immediately upon β-H elimination from methoxy, results in the simultaneous desorption of methanol. The pre-adsorbed atomic oxygen species was completely consumed in the reaction because neither dioxygen nor carbon dioxide were observed desorbing. The water desorption at 170-180 K is due to desorption-limited evolution of water formed by the reaction between pre-adsorbed atomic oxygen species and alcoholic hydrogen atoms of methanol.

Quantitative analysis of TPRS results. The average number of methanol molecules stabilized per methoxy was evaluated by utilizing mass balances for each product via quantitative mass spectrometry of the temperature programmed reaction profiles.[33] Briefly, integrated desorption peak areas were corrected for the ionization cross sections of the parent species and for the sensitivity of the mass spectrometer to the selected ion fragment detected (Supplemental Information). The corrected signals were then calibrated relative to the dioxygen peak obtained from temperature-programmed desorption of a saturation coverage (1.2 ML) of atomic oxygen on Au(110) in order to calculate the absolute amount of each product. The methanol evolved coincident with methyl formate at 225 K can originate either 1) from methanol that was regenerated by recombination of methoxy with hydrogen atoms released in the process of forming methyl formate, or 2) intact methanol stabilized by methoxy. Their ratio can be calculated from the integrated peak areas of methyl formate, methanol, water and dihydrogen, given that formaldehyde production, complete combustion via formate and other decomposition pathways of methoxy were negligible. The initial coverage of 0.05 ML of oxygen atoms (Table 1, line A) reacted with methanol to form two methoxy species per oxygen atom (Table 1, line C), with any residual oxygen reacting with hydrogen atoms released to form water at 225 K (Table 1, line B). Some of the methoxy species coupled to form methyl formate (Table 1, line D) while the rest reacted with hydrogen, regenerating methanol (Table 1, line E). The minimum amount of methanol stabilized by methoxy is then obtained by subtracting the amount of regenerated methanol from the total amount detected (Table 1, line F). These calculations resulted in an average of 1.9 ± 0.3 methanol molecules per methoxy, in good agreement with the 2:1 ratio observed in the STM experiments (below).

Estimating the stabilization energy from peak temperature shift. The stabilization energy of methanol by methoxy was estimated from the increase in desorption temperature relative to methanol adsorbed on clean Au(110), assuming first-order desorption and a constant pre-exponential factor $\boldsymbol{\nu}$ that is independent of coverage, using the Redhead method derived from the Polanyi-Wigner equation:[72]

Table 1. Quantitative analysis of temperature-programmed reaction spectra (Fig. 1) shows stabilization of ~1.9 molecules of methanol per methoxy species. The initial oxygen coverage was 0.05 ML, most of which reacted with methanol, forming methoxy and water, while a fraction (0.01 ML) remained unreacted until 225 K, when it formed water. Some methoxy underwent coupling, producing methyl formate (0.02 ML methyl formate) while the rest (0.04 ML methoxy) regenerated methanol or trace amounts of formaldehyde and formate (not detected by QMS). Accordingly, of the methanol molecules detected at 225 K (0.19 ML), 0.15 ML was intact methanol, which yields 1.9 molecules of methanol stabilized per methoxy species.

Species	Coverage (ML)[*1]
A) Pre-adsorbed atomic oxygen	0.05 (±0.01)
B) Water detected at 225 K	0.01 (±0.003)
C) Methoxy formed at 130 K (2(A-B))	0.08 (±0.01)
D) Methyl formate detected at 225 K	0.02 (±0.004)
E) Remaining methoxy[*2] (C-2D)	0.04 (±0.01)
F) Methanol detected at 225 K	0.19 (±0.02)
G) H_2 detected at 225 K	0.04 (±0.06)
H) Stabilized methanol per methoxy species ((F-E)/C)	1.9 (±0.3)

[*1] The amount of methyl formate, water, dihydrogen and methanol detected were computed from the peak integrals (Supporting Information). Reported here are the sets of mean and standard deviation calculated from data collected in three sets of experiments.

[*2] The amount of methoxy that did not couple must equal the

$$E_d = RT_p\left[ln\left(\frac{\nu T_p}{\beta}\right) - ln\left(\frac{E_d}{RT_p}\right)\right] \quad (10)$$

where E_d is the activation energy, R the gas constant, T_p the peak temperature, and β the heating rate. A pre-exponential factor of 5.8×10^{14} s^{-1} has been measured by heating-rate variation analysis[73,74] for the formation of methyl formate upon linear heating of the Au(110) surface covered with 0.05 ML O/Au(110) and excess methanol.[63] Using this apparent pre-exponential factor value, desorption energies of 0.67 eV and 0.55 eV were computed for desorption at 225 K and 184 K, respectively, yielding a stabilization energy of 0.13 eV (12.1 kJ/mol). This value gives the minimum stabilization energy of methanol molecules by methoxy because the β-H elimination of methoxy triggers desorption of methanol from the stabilized state, i.e. there is nothing to stabilize methanol above its desorption temperature in the absence of methoxy.

Identifying surface-bound intermediates with high-resolution electron energy loss spectroscopy. High resolution energy loss vibrational spectroscopy was employed to verify the surface species existent prior to methyl formate desorption. Upon adsorption of 0.5 ML of methanol on 0.13 ML O/Au(110) at 120 K, the vibrational mode at 335 cm^{-1} assigned to Au-O stretch (ν_{Au_O}) was observed (Fig. 2a). This vibrational frequency was not observed for methanol or for atomic oxygen adsorbed on the clean Au(110) surface (Fig. 2b,c) and is characteristic for alkoxides, confirming the presence of methoxy intermediates on the surface.[75] A broad band was observed between 600-800 cm^{-1} which can be assigned to the bending mode of O— H in methanol (γ_{OH}) and libration mode of water due to the presence of intact methanol and water that formed as a result of methanol activation by atomic oxygen. These two modes were also observed for water and methanol adsorbed on clean Au(110) (Supporting Information). The O — H stretch above 3000 cm^{-1} [76] was not observed, probably because it was obscured by the more intense C— H stretch of methoxy or it was screened by the dipole moments of methoxy species.

When the surface was annealed to 180 K (Fig. 2a), the intensity of the Au-O stretching mode increased and the mode at 600-800 cm^{-1} diminished. The former observation is likely due to the increase in the methoxy coverage by activation of a larger fraction of methanol and/or change in the orientation of the methoxy species into a more up-right configuration. The latter observation is attributed to the reduction in the coverage of adsorbed water because water desorbs from the clean surface below 170 K. Some methanol was still present because the peak did not completely disappear.

Imaging methanol stabilization with scanning tunneling microscopy. In order to further clarify the observed stabilization effect and better understand the nature of methanol-methoxy-substrate interactions at the atomic-scale, STM experiments were conducted.

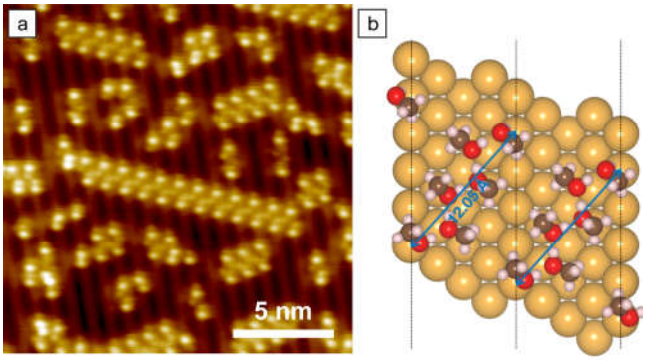

Figure 3. Adsorption structure of methanol at high coverage on pristine Au(110)-(1×2) a) observed by STM and b) optimized by DFT. For the STM experiment 0.3 L of methanol was dosed at 5 K on Au(110), and the sample was annealed at 160 K to equilibrate the surface-bound methanol molecules. Extended chains of methanol running across the rows were observed. Imaging conditions: 0.03 V, 0.01 nA. The DFT-optimized model shows that the methanol chains consist of units of six hydrogen-bonded methanol molecules (length: 12.05 Å) that result in the chains extending diagonally across the $[1\bar{1}0]$

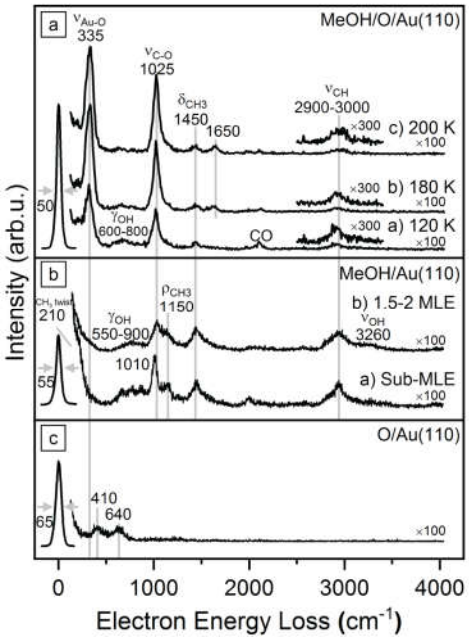

Figure 2. High-resolution electron energy loss (HREELS) spectra showing (a) characteristic vibrational frequencies of intermediates formed from the reaction of 0.5 ML of methanol with 0.13 ML of atomic oxygen on Au(110), (b) vibrational frequencies of methanol on pristine Au(110), and c) vibrational frequencies of 0.07 ML atomic oxygen on pristine Au(110). The formation of methoxy at 120 K is demonstrated by the appearance of an intense Au-O stretch at 335 cm^{-1}. The broad peak between 600-800 cm^{-1} at 120 K is assigned to the bending mode of OH within methanol and the libration mode of water. After annealing to 180 K this peak diminishes due to desorption of water, but does not completely disappear, which suggests that some methanol was still present. Mode assignments can be found in the Supporting Information. All spectra were

Au(110) and Atomic Oxygen on Au(110). Au(110) adopts the "missing row" (1×2) reconstruction, where the (111) microfacets are capped by rows of undercoordinated atoms along the [1$\bar{1}$0] direction (Fig. 3).[77,78] Using atomically resolved STM images to calibrate the Au(110) unit cell, a grid was overlaid onto the STM images and used to identify the binding sites of different intermediates observed on the surface. At a 0.13 ML coverage of atomic oxygen on Au(110), oxygen atoms were imaged as dark features along the [1$\bar{1}$0] direction, in agreement with previous results (Supporting Information).[79,80] The oxygen adsorption sites in the dark areas were identified in the highly resolved STM images as anti-symmetric chains along the [1$\bar{1}$0] direction, in agreement with previous DFT results with an apparent depth of 60 pm, which is also in agreement with previous experimental results.[79,81] Overall, these results confirm the presence of atomic oxygen on the Au(110) surface after ozone exposure.

Methanol on Au(110). Before imaging the interactions of methanol following reaction with preadsorbed O, the adsorption of methanol on pristine Au(110) was studied. After exposing the Au(110) surface to 0.3 L of methanol at 5 K and annealing at 160 K to equilibrate the methanol ensembles, extended chains of methanol molecules were observed running at an angle of 67 degrees across the rows with a few isolated dimers and trimers oriented approximately along the [1$\bar{1}$0] direction (Fig. 3a).

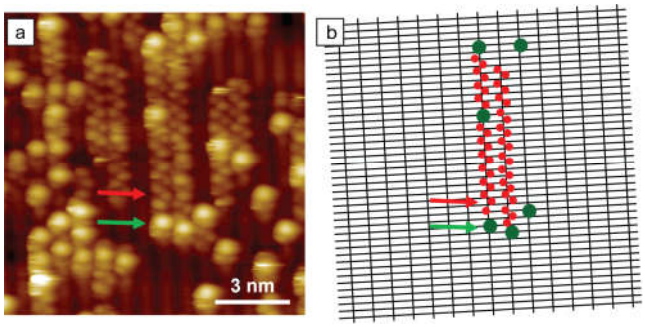

Figure 4. STM image of 0.5 ML of methanol on 0.13 ML of O precovered Au(110) surface acquired at 5 K. (a) Post 180 K anneal, methoxy (green arrow) stabilizes methanol resulting in the formation of methanol chains (red arrow) along the [1$\bar{1}$0] direction on Au(110). Imaging conditions: -0.3 V, 0.005 nA. (b) Au(110)-(1 × 2) reconstruction unit cell grid showing binding sites of the features observed in (a). The underlying Au atoms on the surface lie at the intersections of the grid lines.

0.5 ML Methanol on O/Au(110). Methanol adsorption on an O pre-covered Au(110) surface lead to the formation a different set of structures. An exposure of 0.13 ML of O pre-covered Au(110) to 0.5 ML of methanol at 5 K and subsequent annealing of the surface to 180 K to enable reaction of the methanol with adsorbed oxygen and desorption of water lead to a new set of distinct features (Fig. 4a). The bright circular species highlighted by the green arrow in Fig. 4a and depicted by green circles in Fig. 4b indicate binding in an atop configuration. The dimmer species highlighted by the red arrow in Fig. 4a and modeled by red circles in Fig. 4b form tightly packed anti-symmetric chains that are nearly identical in arrangement to those observed for methanol on the pristine surface, except in this case the chains run along the [1$\bar{1}$0] direction. Vibrational spectroscopy at this annealing temperature reveals the presence of methanol (γO-H mode between 600-800 cm^{-1}) and methoxy (Au-O stretch at 335 cm^{-1}) (Fig. 2). The O-H bending mode between 600-800 cm^{-1} is assigned to methanol because water desorbs readily from the surface at the

annealing temperature. Therefore, the two distinct features observed post 180 K annealing modeled by red and green circles in Fig. 4b can be ascribed to methanol molecules and methoxy intermediates, respectively. In the STM image the ratio of the methanol to methoxy species is roughly 2:1 based on the ratio of the dim (red circles) to bright features (green circles). Adsorbate-induced restructuring of the gold surface from (1×2) to (1×1)[24] was not observed for this system.

Modeling the adsorption structure of methanol network with density functional theory. To better understand the molecular arrangement of methanol molecules within the unit cell of the diagonal methanol structure, chain structures with different numbers of molecules were tested and optimized by DFT. The relative rotational angle of the chain with respect to the substrate was constrained such that it matched closely with the observation in the STM images. The optimized result indicated that the larger network structures consist of units of six hydrogen-bonded methanol molecules with the terminal methanol molecules adsorbed on the top of rows and the four other methanol molecules adsorbed in the troughs (Fig. 3b). The DFT estimated binding energy is -0.66 eV per methanol.

Modeling the adsorption structure of methanol-methoxy network with density functional theory. There are two important questions that were addressed by DFT in order to reach an atomic scale assignment of the STM features to methanol and methoxy. These assignments are also aided by the knowledge of the molecular structure of methanol on the clean surface obtained using scanning tunneling microscopy. These questions are (1) what are the relative intensities of the methoxy and methanol in the STM image, and (2) what are the compared atomic arrangements and stability for the methanol structure along the [1$\bar{1}$0] direction in the presence of methoxy and the rotated orientation observed on the clean surface?

First, DFT simulation of the STM image by well-established methods[82] (see Methods) indicated that methoxy is indeed significantly brighter than methanol on the Au surface (Fig. 5b). Second, the species likely to comprise the complex pattern observed in STM following the anneal to 180 K were assessed as follows. When placed to form a zigzag chain along the Au row, methoxy moieties were found to exhibit appreciable repulsive interactions of 0.20 eV/methoxy. In contrast, methanol molecules exhibited attractive interactions; the adsorption energy of an isolated methanol on the Au surface of -0.39 eV increased to -0.63 eV per methanol molecule for the hydrogen-bonded zigzag methanol chain adsorbed along the top Au(110) row on the otherwise clean surface (Fig. S6). Furthermore, the 2D structure exhibited in the dimmer features closely resembles the condensed phase of methanol on the clean surface, except it is rotated to align with the close packed rows of Au. It is therefore reasonable to assign the features comprising the rather close-packed extended islands in the STM image to methanol chains (Fig. 5). Note that the computed stability of the methanol chains on the clean surface is not very different for the methanol chains on clean surface for either the [1$\bar{1}$0] or the rotated configuration (-0.63 vs -0.66). The DFT calculations reveal that methoxy stabilizes the methanol chain and the adsorption energy per molecule of methanol increases to -0.72 eV (Table 2). Thus, subtle electronic perturbations of the gold by the methoxy could easily lead to reorientation of the methanol chains. Since the assignment of the chains to methanol leaves adsorbed methoxy unaccounted for, the brighter features observed in STM should correspond to a methoxy molecule, in agreement with theory.

DISCUSSION

It is important to put this work into perspective with relationship to previous research of this nature. Aside from the more general studies cited in the introduction, there has been considerable fundamental research on the interaction of water, the most common solvent, with metals and metal oxide surfaces. Early studies showed that (1) on clean Ag(110) adsorbed water forms clusters at 100 K, and (2) water reacts quantitatively with preadsorbed atomic oxygen on to form adsorbed hydroxyl, which stabilizes adsorbed water by up to 4.3 kcal/mol, both effects being due to H-

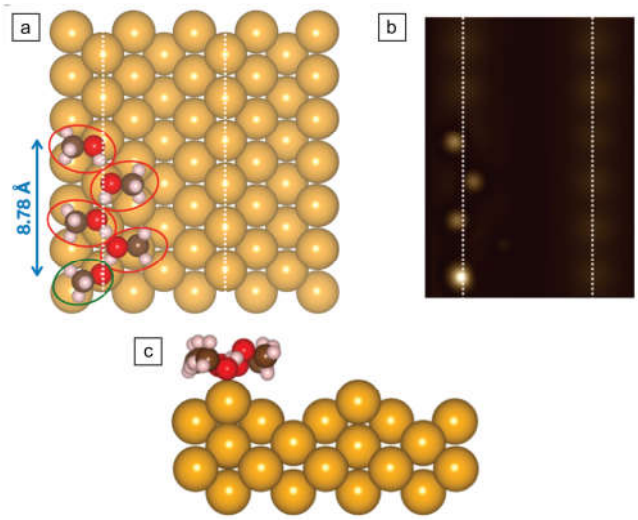

Figure 5. DFT optimized co-adsorption structure of a methanol zigzag chain and methoxy intermediate along the Au(110) top row. (a) In the plan view the methanol molecules are marked by red circles and methoxy by a green circle. (b) The associated STM image for the structure shown in (a) was simulated using the electronic states with energies ranging from the Fermi level to +40 mV (constant height, z=5.96 Å). (c) Side view of the structure. The Au rows along the [1$\bar{1}$0] direction are marked by white lines in (a) and (b).

Table 2. Adsorption energies of methanol at different configurations along the Au row.

	methanol monomer	methoxy-stabilized methanol monomer	methanol tetramer	methoxy-stabilized tetramer
Adsorption energy				

bonding.[39–41] Subsequent work shows that the adsorbed OH forms ordered structures along the [1$\bar{1}$0] direction.[42,43] Similar OH structures form on Cu(110).[44] Thus, hydrogen bonded structures can be expected for water on clean metal surfaces.

Similar effects are seen on metal oxide surfaces.[38] Titania single crystal surfaces have proved especially fruitful for STM studies of water adsorption,[83–97] but similar effects have been reported for other oxides as well.[38,98,99] In general, water undergoes partial dissociation on defect sites (although there have been debates that defect-free surfaces may also dissociate water), forming OH, in some cases via water dimers, and excess water may cluster around the OH at low temperature, indicative of stabilization via H-bonding.

The results reported here demonstrate that methanol-methoxy interactions lead to extended hydrogen-bonded structures on clean gold surfaces. Surface-bound methoxy species, when formed by reacting methanol with preadsorbed oxygen atoms, are surrounded by unreacted, intact methanol molecules that are stabilized well beyond their desorption temperature from the clean surface until methoxy undergoes β-H elimination (the rate-determining step) to form methyl formate (~225 K). Specifically, methanol desorbs at 170-190 K in the absence of methoxy species, which clearly shows that methanol is stabilized on the surface by the methoxy species. The origin of this effect, supported by DFT calculations, is that methanol molecules hydrogen-bond with the anchoring oxygen atom of methoxy species. This effect is much more pronounced than the effect of OH on water desorption from Ag(110), where water desorbs well below the temperature at which OH disproportionates.

While the methanol molecules form hydrogen-bonded networks consisting of units of six methanol molecules oriented diagonally across the top rows of clean Au(110) in the absence of adsorbed methoxy, methoxy causes the methanol network to reorient and propagate along the rows. Side-by-side comparison of the two structures (Figs. 6, S6) and hydrogen-bonding distances (Fig. S6) shows that the arrangements of the methanol molecules are nearly identical in the two structures. The adsorption energy of methanol on the pristine Au(110) was calculated to be -0.66 eV per methanol in the diagonal configuration, which is insignificantly more stable than the value calculated were the chains to be oriented along the close-packed rows of Au on the clean surface (-0.63 eV per methanol). The difference between the two adsorption energies is insignificant as DFT does not have this level of accuracy. Despite the small energetic difference calculated, methanol on the clean surface obviously prefers to be oriented 67 degrees from the close-packed direction. This fact illustrates that the structure of methanol on the clean surface is dictated by small energy differences. Moreover, the difference in adsorption energy induced by methoxy is sufficient to reorient the methanol clusters due to the stabilization provided by local hydrogen bonding interactions with the methoxy.

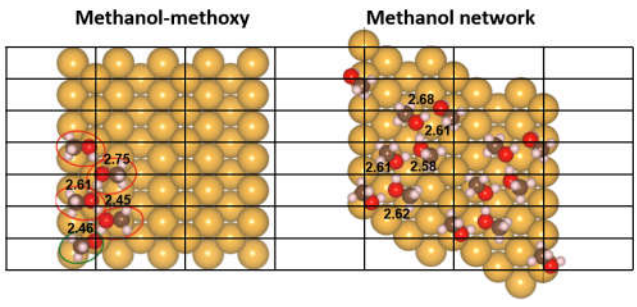

Figure 6. Au(110)-(1 × 2) reconstruction unit cell grid overlayed on top of DFT-optimized binding sites of methoxy-stabilized methanol network and methanol network. The neighboring oxygen-oxygen distances are shown (in Å). Comparison between the binding sites demonstrates that the arrangements are nearly identical. The underlying Au atoms on the surface lie at the intersections of the grid lines.

Looking closely at the distribution of methanol and methoxy observed in STM images, the following observations can be made. At low coverages on pristine Au(110), oxygen atoms form short, zig-zag chains across the Au rows which condense into two-dimensional patches at higher coverages.[79] STM reveals that most of the methoxy species are also clumped, appearing to reflect the ordering of pre-adsorbed O. This result suggests that either methoxy species are not mobile below 180 K or they exhibit attractive interactions with one another when located *across* the rows. If methoxy species *were* isolated from each other, they would be expected to stabilize even more methanol molecules.

It is also important to note the arrangement of methanol present even as the surface approaches saturation coverage. At a local surface coverage of 0.7 ML shown in Fig. 4 most of the adsorbed methanol is found in chains that contain at least one methoxy. However, chains also appear that include no methoxys. Remarkably, this "untethered" methanol does not desorb at 184 K, but is stabilized by the surrounding methanol. These long chains consisting of several methanol molecules do not desorb until methoxy reacts further, indicating that the effect of local hydrogen bonding between methoxy and methanol is propagated along the chains and is not simply a local effect. In general, the degree to which the chains may differ from that observed on the clean surface depends on the surface concentration of methoxy. Locally the untethered methanol is trapped by the methoxy-anchored chains. This effect would be expected to dominate unless the methoxy concentration were so low that the free surface dominates. Under such conditions there would be insufficient methoxy, and the effect would become minimal. Expressed differently, when methoxy is adsorbed on the surface, it serves as the seed for the methanol chain to grow along the rows. These seeds reduce the mobility of even the methanol molecules that do not directly interact with the methoxy and therefore prevent them from forming clusters that span across Au rows.

Previous studies have alluded to methanol stabilization by methoxy on the Au(111) and Ag(110) surfaces. For the *Au(111)* surface an increase in the desorption temperature

of methanol in oxidative self-coupling has been reported,[60] and it was ascribed to either recombination of methoxy and hydrogen atoms (disproponation) or stabilization by oxygen atoms in the work. However, according to our evaluation there was too much methanol desorption to be the result of disproptionation or stabilization by unreacted oxygen.[100] Similarly, for the *Ag(110)* surface it was suggested that methanol was stabilized by methoxy.[71] We conclude that the temperature shift observed on the Au(111) and the enhanced adsorption on Ag(110) may be due to the same stabilization effect of methoxy species.

Between the (111) surface and (110) surface, some structural sensitivity of the stabilization effect and molecular arrangement is expected. For example, the vdW-induced stabilization for methoxy, ethoxy, 1-propoxy, 2-propoxy, and benzyl alkoxy due to interaction of the pendant group of the alkoxy is larger on the Au(110) surface than on Au(111)[22] due to the ability of molecules to tilt toward the protrusions of the more corrugated 2x1 reconstructed Au(110) surface, which optimizes the vdW attraction to the surface. Furthermore, on close-packed Au(111), methanol, for example, forms hexamers with a ring structure or a slightly less stable chain structures along the $\sqrt{3}$ direction,[51,54] which are different from the structures observed on the Au(110) surface. These findings suggest that the structure of hydrogen-bonded networks between methoxy and methanol are expected to be different between the (110) surface and other surfaces.

One important question that remains to be addressed is how formation of this methoxy-methanol complex affects the kinetics of the successive steps involved in coupling, e.g., methanol desorption, β-H elimination from methoxy and nucleophilic attack on the resulting formaldehyde by methoxy, both in the temperature programmed reaction and steady state modes of operation. The most stable adsorption site of isolated methoxy was determined to be the bridge-site on the top-most row in the work reported here and in prior work.[22] For the methanol-methoxy complex, however, methoxy appears to bind in an atop configuration. This reorientation may change important factors such as the Au-O bond strength and the distance between the methyl group and surface atoms, thereby affecting the rates of the β-H elimination step, which is the rate-determining step of the coupling reaction. It has been well-established that solvation of initial states and transition states greatly affects the activation barrier height and hence the reactions rates.[26,29,57,58,101–103] This issue becomes even more important when studying the selectivity of *cross*-coupling reactions. The number of solvating alcohols and the strength of hydrogen-bonding would likely depend on the nature of the alkyl chains, and the coupling involving alkoxides that experience stronger solvation effects may be sterically hindered by a greater extent than other alkoxides that are more isolated. Due to these extended lateral interactions, in principle, effects on the rate constants for elementary steps would be expected. One notable example is the effect on the surface lifetime of adsorbed methanol due to association with the methoxy. The rate constant parameters (ν, E) for methanol from the clean surface and from the methoxy stabilized structure are 3.1×10^{17} s^{-1}, 63.0 kJ/mol (Fig. S8) and 5.8×10^{14} s^{-1}, 64.4 kJ/mol,[63] respectively. These differences increase the surface lifetime of methanol in the presence or methoxy by approximately three orders of magnitude. Such effects can alter steady state rates of conversion significantly.

To assess the effect of solvation of the methoxy by surrounding methanol molecules the kinetics of C-H bond activation in the methoxy were studied by temperature-programmed reaction spectroscopy at varying methanol to methoxy ratios (Figs. S7, S8). When the initial oxygen coverage was fixed at 0.05 ML and methanol exposures of 1 L and 2.5 L were tested, a slight increase (<+5 K) in the peak temperature for methyl formate evolution/methanol desorption was observed for the higher methanol dose. At the highest exposure of methanol an excess of 0.16 ML of molecular methanol was detected with the evolution of methyl formate while no measurable excess was detected for the lowest methanol dose. While the effect is small, this observed increase in the decomposition temperature of methoxy suggest that the presence of solvating methanol molecules does increase the barrier for the β-H abstraction process. It is possible that both the reactant and transition states are similarly affected by the surrounding methanol. However, it is important to note that the methoxy has a very large effect on the rate constant for desorption of methanol.

Additionally, while the observations reported here were made under ultrahigh vacuum conditions, they suggest an effect that may contribute to the dramatic difference in selectivity observed for cross coupling between methanol and propanol in the liquid and gas phases.[104] Specifically, in the gas-phase, propoxy intermediate is more stable compared to methoxy species because of the Au-alkyl van der Waals interactions, resulting in the dominance of the adsorbed propoxy on the surface, yielding propyl propionate as the dominant product. In order to form significant amount of propyl formate very high concentrations of methanol in the gas phase are required. However, catalysis of the cross coupling in the liquid phase mitigates this effect, and high selectivity for the cross coupled product can be achieved at equimolar concentrations. This fact suggests that solvation of the alkoxy intermediates by reactant alcohols may neutralize the preferential stabilization of longer alkoxide species on the surface. We anticipate the effect reported here to be present in many catalytic reactions that involve solvents that are capable of hydrogen-bonding.

The reactant-intermediate stabilization effects observed in this work may be quite general, particularly for reactions with molecules and reaction intermediates capable of hydrogen bonding. It is well-known that solvents affect liquid-phase heterogeneous catalysis, potentially by directly participating in the reactions, changing the stability of reactants, intermediates, transition states, and products, and/or by reducing the density of active sites by competitive adsorption with the reactants and intermediates.[8–10] While the work reported here shows the stabilization of

methanol by adsorbed methoxy species, recent works using STM have demonstrated that hydration changes the ordering of other adsorbates including 4, 4′-dihydroxy azobenzene[45] and 3-methoxy-9-fluorene[46] on Ag(111) and bitartrate on Cu(110).[12] We have also observed stabilization of water by surface-bound acetate on Au(110) by c.a. 10 kJ/mol (increase in desorption temperature by 40 K) and weakening of the Au-O bond of acetate.[74]

The stabilization effects reported in this work may also be important in other liquid/surface reaction systems where surface-bound species interact with the solvent in such a way as to change the structure of the adsorbed solvent and, consequently, the near-surface structure of the solvent. One such area is electrochemistry, one of the fields that have seen significant developments in the past few decades owing to the need for more efficient renewable energy harvesting and storage systems. Researchers have studied the molecular-scale ordering and elementary reaction steps occurring in the electric double later (EDL),[105] because the structure of the interfacial water in the EDL can have significant effects on the performance of electrochemical systems.[106–108] For example, it has been shown that the orientation of water molecules and hence the hydrogen bonding network in EDLs changes upon application of negative bias on gold electrodes, using x-ray adsorption spectroscopy (XAS) and *ab initio* molecular dynamics (AIMD) simulations for the case of Au film deposited on a Si_3N_4 membrane[109] and using *in situ* Raman spectroscopy and AIMD for Au(111).[110] Another study revealed that the EDL formed at a polycrystalline platinum electrode in aqueous sulfuric acid is dominated by sulfate ions (SO_4^{2-}), hydronium ions (H_3O^+) and solvating water, and the adsorption and accumulation of sulfate ions at the interface alters the hydrogen-bonding network of interfacial water molecules.[111] In general, our results provide experimental evidence that the arrangement of adsorbed species may be altered by hydrogen-bonded networks at the solid/liquid (gas) interfaces, and it may be necessary to include such effects in theoretical models related to activity and selectivity of heterogeneous catalytic reactions as well as electrochemical reactions.

CONCLUSIONS

In conclusion, extended hydrogen bonding networks have been identified that originate from the interactions between reaction intermediates and reactants involved in the oxidative coupling of methanol on Au(110). These interactions significantly stabilize the adsorbed reactant molecule to the extent that they form a solvating network up to the temperature at which reaction of the intermediate commences. Detailed examination reveals stabilization of clusters of methanol by interspersed methoxy intermediates. Notably, the presence of methoxy changes the adsorption structure of and increases the binding energy of methanol on Au(110). The increased stability of the adsorbed methanol appears to be due to hydrogen bonding interactions with methoxy intermediates that effects the structure of the reactant-intermediate complex over several lattice units across the surface. These results underscore the fact that such interactions between reaction intermediates and reactants *may* be present in many other heterogeneously catalyzed reactions and that they may need to be included in theoretical treatments of reaction rates and kinetics, particularly in the liquid phase.

ASSOCIATED CONTENT

Supporting Information
Details of TPD/TPRS, additional STM images and DFT results (PDF)
This material is available free of charge via the Internet at http://pubs.acs.org.

AUTHOR INFORMATION

Corresponding Author

Robert J. Madix - John A. Paulson School of Engineering and Applied Sciences, Harvard University, Cambridge, MA 02138, USA
Email: rmadix@seas.harvard.edu

Author Contributions

‡These authors contributed equally.

Notes

The authors declare no competing financial interest.

ACKNOWLEDGMENTS

This work was supported as part of the Integrated Mesoscale Architectures for Sustainable Catalysis (IMASC), an Energy Frontier Research Center funded by the US Department of Energy (DOE), Office of Science, Basic Energy Sciences (BES), under award no. DE-SC0012573. W. C. used resources of the Center for Functional Nanomaterials, which is a U.S. Department of Energy (DOE) Office of Science facility, and the Scientific Data and Computing Center, a component of the BNL Computational Science Initiative, at BNL (contract no. DE-SC0012704). E. M. gratefully acknowledges the Ito Foundation for financial support.

REFERENCES

(1) Wescott, C. R.; Klibanov, A. M. The Solvent Dependence of Enzyme Specificity. *Biochim. Biophys. Acta (BBA)/Protein Struct. Mol.* **1994**, *1206* (1), 1–9.

(2) Sui, Y.; Ji, X. Anticatalytic Strategies to Suppress Water Electrolysis in Aqueous Batteries. *Chem. Rev.* **2021**, *121* (11), 6654–6695.

(3) Prins, L. J.; Reinhoudt, D. N.; Timmerman, P. Noncovalent Synthesis Using Hydrogen Bonding. *Angew. Chemie Int. Ed.* **2001**, *40* (13), 2382–2426.

(4) Barth, J. V.; Costantini, G.; Kern, K. Engineering Atomic and Molecular Nanostructures at Surfaces. *Nature* **2005**, *437*, 671–679.

(5) Cleland, W. W.; Frey, P. A.; Gerlt, J. A. The Low Barrier Hydrogen Bond in Enzymatic Catalysis. *J. Biol. Chem.* **1998**, *273* (40), 25529–25532.

(6) Haw, J. F.; Xu, T.; Nicholas, J. B.; Goguen, P. W. Solvent-Assisted Proton Transfer in Catalysis by Zeolite Solid Acids.

Nature **1997**, *389*, 832–835.
(7) Chang, C. R.; Huang, Z. Q.; Li, J. The Promotional Role of Water in Heterogeneous Catalysis: Mechanism Insights from Computational Modeling. *Wiley Interdiscip. Rev. Comput. Mol. Sci.* **2016**, *6* (6), 679–693.
(8) Sievers, C.; Scott, S. L.; Noda, Y.; Qi, L.; Albuquerque, E. M.; Rioux, R. M. Phenomena Affecting Catalytic Reactions at Solid–Liquid Interfaces. *ACS Catal.* **2016**, *6* (12), 8286–8307.
(9) Saleheen, M.; Heyden, A. Liquid-Phase Modeling in Heterogeneous Catalysis. *ACS Catal.* **2018**, *8* (3), 2188–2194.
(10) Potts, D. S.; Bregante, D. T.; Adams, J. S.; Torres, C.; Flaherty, D. W. Influence of Solvent Structure and Hydrogen Bonding on Catalysis at Solid-Liquid Interfaces. *Chem. Soc. Rev.* **2021**, *50* (22), 12308–12337.
(11) Ulman, A. Formation and Structure of Self-Assembled Monolayers. *Chem. Rev.* **1996**, *96* (4), 1533–1554.
(12) Lin, C.; Darling, G. R.; Forster, M.; McBride, F.; Massey, A.; Hodgson, A. Hydration of a 2D Supramolecular Assembly: Bitartrate on Cu(110). *J. Am. Chem. Soc.* **2020**, *142* (32), 13814–13822.
(13) Castillo, H. D.; Yang, J.; Debnath, S.; Dobscha, J. R.; Trainor, C. Q.; Mortensen, R. D.; Raghavachari, K.; Flood, A. H.; Ortoleva, P. J.; Tait, S. L. Solution-Mediated Annealing Pathways Are Critical for Supramolecular Ordering of Complex Macrocycles at Surfaces. *J. Phys. Chem. C* **2020**, *124* (12), 6689–6699.
(14) Birdja, Y. Y.; Pérez-Gallent, E.; Figueiredo, M. C.; Göttle, A. J.; Calle-Vallejo, F.; Koper, M. T. M. Advances and Challenges in Understanding the Electrocatalytic Conversion of Carbon Dioxide to Fuels. *Nat. Energy* **2019**, *4*, 732–745.
(15) Aetukuri, N. B.; McCloskey, B. D.; García, J. M.; Krupp, L. E.; Viswanathan, V.; Luntz, A. C. Solvating Additives Drive Solution-Mediated Electrochemistry and Enhance Toroid Growth in Non-Aqueous Li–O_2 Batteries. *Nat. Chem.* **2015**, *7*, 50–56.
(16) Burke, C. M.; Pande, V.; Khetan, A.; Viswanathan, V.; McCloskey, B. D. Enhancing Electrochemical Intermediate Solvation through Electrolyte Anion Selection to Increase Nonaqueous Li-O_2 Battery Capacity. *Proc. Natl. Acad. Sci. U. S. A.* **2015**, *112* (30), 9293–9298.
(17) Abild-Pedersen, F.; Greeley, J.; Studt, F.; Rossmeisl, J.; Munter, T. R.; Moses, P. G.; Skúlason, E.; Bligaard, T.; Nørskov, J. K. Scaling Properties of Adsorption Energies for Hydrogen-Containing Molecules on Transition-Metal Surfaces. *Phys. Rev. Lett.* **2007**, *99* (1), 016105.
(18) Nørskov, J. K.; Bligaard, T.; Rossmeisl, J.; Christensen, C. H. Towards the Computational Design of Solid Catalysts. *Nat. Chem.* **2009**, *1*, 37–46.
(19) Kitchin, J. R.; Nørskov, J. K.; Barteau, M. A.; Chen, J. G. Role of Strain and Ligand Effects in the Modification of the Electronic and Chemical Properties of Bimetallic Surfaces. *Phys. Rev. Lett.* **2004**, *93* (15), 156801.
(20) Wang, T.; Ibañez, J.; Wang, K.; Fang, L.; Sabbe, M.; Michel, C.; Paul, S.; Pera-Titus, M.; Sautet, P. Rational Design of Selective Metal Catalysts for Alcohol Amination with Ammonia. *Nat. Catal.* **2019**, *2*, 773–779.
(21) Rodriguez-Reyes, J. C. F.; Siler, C. G. F.; Liu, W.; Tkatchenko, A.; Friend, C. M.; Madix, R. J. Van Der Waals Interactions Determine Selectivity in Catalysis by Metallic Gold. *J. Am. Chem. Soc.* **2014**, *136* (38), 13333–13340.
(22) Karakalos, S.; Xu, Y.; Cheenicode Kabeer, F.; Chen, W.; Rodríguez-Reyes, J. C. F.; Tkatchenko, A.; Kaxiras, E.; Madix, R. J.; Friend, C. M. Noncovalent Bonding Controls Selectivity in Heterogeneous Catalysis: Coupling Reactions on Gold. *J. Am. Chem. Soc.* **2016**, *138* (46), 15243–15250.
(23) O'Connor, C. R.; Hiebel, F.; Chen, W.; Kaxiras, E.; Madix, R. J.; Friend, C. M. Identifying Key Descriptors in Surface Binding: Interplay of Surface Anchoring and Intermolecular Interactions for Carboxylates on Au(110). *Chem. Sci.* **2018**, *9* (15), 3759–3766.
(24) Hiebel, F.; Shong, B.; Chen, W.; Madix, R. J.; Kaxiras, E.; Friend, C. M. Self-Assembly of Acetate Adsorbates Drives Atomic Rearrangement on the Au(110) Surface. *Nat. Commun.* **2016**, *7*, 13139.
(25) Zhi, Y.; Shi, H.; Mu, L.; Liu, Y.; Mei, D.; Camaioni, D. M.; Lercher, J. A. Dehydration Pathways of 1-Propanol on HZSM-5 in the Presence and Absence of Water. *J. Am. Chem. Soc.* **2015**, *137* (50), 15781–15794.
(26) Zhao, Z.; Bababrik, R.; Xue, W.; Li, Y.; Briggs, N. M.; Nguyen, D. T.; Nguyen, U.; Crossley, S. P.; Wang, S.; Wang, B.; Resasco, D. E. Solvent-Mediated Charge Separation Drives Alternative Hydrogenation Path of Furanics in Liquid Water. *Nat. Catal.* **2019**, *2*, 431–436.
(27) Bregante, D. T.; Johnson, A. M.; Patel, A. Y.; Ayla, E. Z.; Cordon, M. J.; Bukowski, B. C.; Greeley, J.; Gounder, R.; Flaherty, D. W. Cooperative Effects between Hydrophilic Pores and Solvents: Catalytic Consequences of Hydrogen Bonding on Alkene Epoxidation in Zeolites. *J. Am. Chem. Soc.* **2019**, *141* (18), 7302–7319.
(28) Zare, M.; Saleheen, M.; Kundu, S. K.; Heyden, A. Dependency of Solvation Effects on Metal Identity in Surface Reactions. *Commun. Chem.* **2020**, *3*, 187.
(29) Li, G.; Wang, B.; Resasco, D. E. Water-Mediated Heterogeneously Catalyzed Reactions. *ACS Catal.* **2020**, *10* (2), 1294–1309.
(30) Cheng, G.; Jentys, A.; Gutiérrez, O. Y.; Liu, Y.; Chin, Y.-H.; Lercher, J. A. Critical Role of Solvent-Modulated Hydrogen-Binding Strength in the Catalytic Hydrogenation of Benzaldehyde on Palladium. *Nat. Catal.* **2021**, *4*, 976–985.
(31) Ebbesen, S. D.; Mojet, B. L.; Lefferts, L. In Situ ATR-IR Study of CO Adsorption and Oxidation over Pt/Al_2O_3 in Gas and Aqueous Phase: Promotion Effects by Water and pH. *J. Catal.* **2007**, *246* (1), 66–73.
(32) Hidalgo-Carrillo, J.; Aramendía, M. A.; Marinas, A.; Marinas, J. M.; Urbano, F. J. Support and Solvent Effects on the Liquid-Phase Chemoselective Hydrogenation of Crotonaldehyde over Pt Catalysts. *Appl. Catal. A Gen.* **2010**, *385* (1–2), 190–200.
(33) Akpa, B. S.; D'Agostino, C.; Gladden, L. F.; Hindle, K.; Manyar, H.; McGregor, J.; Li, R.; Neurock, M.; Sinha, N.; Stitt, E. H.; Weber, D.; Zeitler, J. A.; Rooney, D. W. Solvent Effects in the Hydrogenation of 2-Butanone. *J. Catal.* **2012**, *289*, 30–41.
(34) Yoon, Y.; Rousseau, R.; Weber, R. S.; Mei, D.; Lercher, J. A. First-Principles Study of Phenol Hydrogenation on Pt and Ni Catalysts in Aqueous Phase. *J. Am. Chem. Soc.* **2014**, *136* (29), 10287–10298.
(35) Behtash, S.; Lu, J.; Faheem, M.; Heyden, A. Solvent Effects on the Hydrodeoxygenation of Propanoic Acid over Pd(111) Model Surfaces. *Green Chem.* **2014**, *16* (2), 605–616.
(36) Wan, H.; Vitter, A.; Chaudhari, R. V.; Subramaniam, B. Kinetic Investigations of Unusual Solvent Effects during Ru/C Catalyzed Hydrogenation of Model Oxygenates. *J. Catal.* **2014**, *309*, 174–184.
(37) Bodenschatz, C. J.; Sarupria, S.; Getman, R. B. Molecular-Level Details about Liquid H_2O Interactions with CO and Sugar Alcohol Adsorbates on Pt(111) Calculated Using Density Functional Theory and Molecular Dynamics. *J. Phys. Chem. C* **2015**, *119* (24), 13642–13651.
(38) Mu, R.; Zhao, Z. J.; Dohnálek, Z.; Gong, J. Structural Motifs of Water on Metal Oxide Surfaces. *Chem. Soc. Rev.* **2017**, *46* (7), 1785–1806.
(39) Stuve, E. M.; Madix, R. J.; Sexton, B. A. The Adsorption and Reaction of H_2O on Clean and Oxygen Covered Ag(110). *Surf. Sci.* **1981**, *111* (1), 11–25.
(40) Bange, K.; Madey, T. E.; Sass, J. K.; Stuve, E. M. The Adsorption of Water and Oxygen on Ag(110): A Study of the Interactions among Water Molecules, Hydroxyl Groups, and Oxygen Atoms. *Surf. Sci.* **1987**, *183* (3), 334–362.
(41) Lim, D. S.-W.; Stuve, E. . Solvation and Ionization of Hydroxyl Groups in Water–Ice Layers on Silver (110). *Surf. Sci.* **1999**, *425* (2–3), 233–244.
(42) Savio, L.; Smerieri, M.; Vattuone, L.; Gussoni, A.; Tassistro,

C.; Rocca, M. STM Study of Hydroxyl Formation at O/Ag(110). *Phys. Rev. B* **2006**, *74* (23), 235412.
(43) Guillemot, L.; Bobrov, K. On the Formation of OH Ordered Layers by Dissociation of H_2O on an Oxygen Covered Ag(110) Surface: An STM Investigation. *Surf. Sci.* **2007**, *601* (3), 871–875.
(44) Lee, J.; Sorescu, D. C.; Jordan, K. D.; Yates, J. T. Hydroxyl Chain Formation on the Cu(110) Surface: Watching Water Dissociation. *J. Phys. Chem. C* **2008**, *112* (45), 17672–17677.
(45) Henzl, J.; Boom, K.; Morgenstern, K. Influence of Water on Supra-Molecular Assembly of 4, 4′-Dihydroxy Azobenzene on Ag(111). *J. Chem. Phys.* **2015**, *142* (10), 101920.
(46) Lucht, K.; Trosien, I.; Sander, W.; Morgenstern, K. Imaging the Solvation of a One-Dimensional Solid on the Molecular Scale. *Angew. Chemie - Int. Ed.* **2018**, *57* (50), 16334–16338.
(47) Michel, C.; Auneau, F.; Delbecq, F.; Sautet, P. C-H versus O-H Bond Dissociation for Alcohols on a Rh(111) Surface: A Strong Assistance from Hydrogen Bonded Neighbors. *ACS Catal.* **2011**, *1* (10), 1430–1440.
(48) Michel, C.; Göltl, F.; Sautet, P. Early Stages of Water/Hydroxyl Phase Generation at Transition Metal Surfaces - Synergetic Adsorption and O-H Bond Dissociation Assistance. *Phys. Chem. Chem. Phys.* **2012**, *14* (44), 15286–15290.
(49) Michel, C.; Zaffran, J.; Ruppert, A. M.; Matras-Michalska, J.; Jędrzejczyk, M.; Grams, J.; Sautet, P. Role of Water in Metal Catalyst Performance for Ketone Hydrogenation: A Joint Experimental and Theoretical Study on Levulinic Acid Conversion into Gamma-Valerolactone. *Chem. Commun.* **2014**, *50* (83), 12450–12453.
(50) Dumon, A. S.; Wang, T.; Ibañez, J.; Tomer, A.; Yan, Z.; Wischert, R.; Sautet, P.; Pera-Titus, M.; Michel, C. Direct n-Octanol Amination by Ammonia on Supported Ni and Pd Catalysts: Activity is Enhanced by "Spectator" Ammonia Adsorbates. *Catal. Sci. Technol.* **2018**, *8* (2), 611–621.
(51) Lawton, T. J.; Carrasco, J.; Baber, A. E.; Michaelides, A.; Sykes, E. C. H. Visualization of Hydrogen Bonding and Associated Chirality in Methanol Hexamers. *Phys. Rev. Lett.* **2011**, *107* (25), 256101.
(52) Baber, A. E.; Lawton, T. J.; Sykes, E. C. H. Hydrogen-Bonded Networks in Surface-Bound Methanol. *J. Phys. Chem. C* **2011**, *115* (18), 9157–9163.
(53) Lawton, T. J.; Carrasco, J.; Baber, A. E.; Michaelides, A.; Sykes, E. C. H. Hydrogen-Bonded Assembly of Methanol on Cu(111). *Phys. Chem. Chem. Phys.* **2012**, *14* (33), 11846–11852.
(54) Murphy, C. J.; Carrasco, J.; Lawton, T. J.; Liriano, M. L.; Baber, A. E.; Lewis, E. A.; Michaelides, A.; Sykes, E. C. H. Structure and Energetics of Hydrogen-Bonded Networks of Methanol on Close Packed Transition Metal Surfaces. *J. Chem. Phys.* **2014**, *141*, 014701.
(55) Feaster, J. T.; Shi, C.; Cave, E. R.; Hatsukade, T.; Abram, D. N.; Kuhl, K. P.; Hahn, C.; Nørskov, J. K.; Jaramillo, T. F. Understanding Selectivity for the Electrochemical Reduction of Carbon Dioxide to Formic Acid and Carbon Monoxide on Metal Electrodes. *ACS Catal.* **2017**, *7* (7), 4822–4827.
(56) Bohra, D.; Ledezma-Yanez, I.; Li, G.; de Jong, W.; Pidko, E. A.; Smith, W. A. Lateral Adsorbate Interactions Inhibit $HCOO^-$ while Promoting CO Selectivity for CO_2 Electrocatalysis on Silver. *Angew. Chemie Int. Ed.* **2019**, *58* (5), 1345–1349.
(57) Chen, B. W. J.; Mavrikakis, M. Formic Acid: A Hydrogen-Bonding Cocatalyst for Formate Decomposition. *ACS Catal.* **2020**, *10* (19), 10812–10825.
(58) Chen, B. W. J.; Bhandari, S.; Mavrikakis, M. Role of Hydrogen-Bonded Bimolecular Formic Acid-Formate Complexes for Formic Acid Decomposition on Copper: A Combined First-Principles and Microkinetic Modeling Study. *ACS Catal.* **2021**, *11* (7), 4349–4361.
(59) Outka, D. A.; Madix, R. J. Brønsted Basicity of Atomic Oxygen on the Au(110) Surface: Reactions with Methanol, Acetylene, Water, and Ethylene. *J. Am. Chem. Soc.* **1987**, *109* (6), 1708–1714.
(60) Gong, J.; Flaherty, D. W.; Ojifinni, R. A.; White, J. M.; Mullins, C. B. Surface Chemistry of Methanol on Clean and Atomic Oxygen Pre-Covered Au(111). *J. Phys. Chem. C* **2008**, *112* (14), 5501–5509.
(61) Xu, B.; Liu, X.; Haubrich, J.; Friend, C. M. Vapour-Phase Gold-Surface-Mediated Coupling of Aldehydes with Methanol. *Nat. Chem.* **2009**, *2*, 61–65.
(62) Xu, B.; Liu, X.; Haubrich, J.; Madix, R. J.; Friend, C. M. Selectivity Control in Gold-Mediated Esterification of Methanol. *Angew. Chemie Int. Ed.* **2009**, *48* (23), 4206–4209.
(63) Xu, Y. Fundamental Studies of Alcohol Reactions on Gold and Copper, Harvard University, 2017.
(64) Madix, R. J. Through the Labyrinth of Surface Reaction Mechanism: A Personal Account, 1964–1992. *Surf. Sci.* **1994**, *299–300*, 785–797.
(65) Gottfried, J. M.; Schmidt, K. J.; Schroeder, S. L. M.; Christmann, K. Oxygen Chemisorption on Au(110)-(1×2) I. Thermal Desorption Measurements. *Surf. Sci.* **2003**, *525* (1–3), 184–196.
(66) Kresse, G.; Furthmüller, J. Efficient Iterative Schemes for Ab Initio Total-Energy Calculations Using a Plane-Wave Basis Set. *Phys. Rev. B* **1996**, *54* (16), 11169–11186.
(67) Joubert, D. From Ultrasoft Pseudopotentials to the Projector Augmented-Wave Method. *Phys. Rev. B* **1999**, *59* (3), 1758–1775.
(68) Perdew, J. P.; Burke, K.; Ernzerhof, M. Generalized Gradient Approximation Made Simple. *Phys. Rev. Lett.* **1996**, *77* (18), 3865–3868.
(69) Tkatchenko, A.; Scheffler, M. Accurate Molecular Van Der Waals Interactions from Ground-State Electron Density and Free-Atom Reference Data. *Phys. Rev. Lett.* **2009**, *102* (7), 073005.
(70) Momma, K.; Izumi, F. VESTA 3 for Three-Dimensional Visualization of Crystal, Volumetric and Morphology Data. *J. Appl. Crystallogr.* **2011**, *44* (6), 1272–1276.
(71) Wachs, I. E.; Madix, R. J. The Oxidation of Methanol on a Silver (110) Catalyst. *Surf. Sci.* **1978**, *76* (2), 531–558.
(72) Redhead, P. A. Thermal Desorption of Gases. *Vacuum* **1962**, *12* (4), 203–211.
(73) Falconer, J. L.; Madix, R. J. Flash Desorption Activation Energies: DCOOH Decomposition and CO Desorption from Ni (110). *Surf. Sci.* **1975**, *48* (2), 393–405.
(74) Muramoto, E.; Robert, J. M. Stabilization of Water by Surface-Bound Acetate and the Effect on Acetate-Au Binding. *J. Phys. Chem. C* In Preparation.
(75) Sexton, B. A.; Hughes, A. E.; Avery, N. R. Surface Intermediates in the Reaction of Methanol, Formaldehyde and Methyl Formate on Copper (110). *Appl. Surf. Sci.* **1985**, *22–23*, 404–414.
(76) Quiller, R. G.; Baker, T. A.; Deng, X.; Colling, M. E.; Min, B. K.; Friend, C. M. Transient Hydroxyl Formation from Water on Oxygen-Covered Au(111). *J. Chem. Phys.* **2008**, *129* (6), 064702.
(77) Binnig, G.; Rohrer, H.; Gerber, C.; Weibel, E. (111) Facets as the Origin of Reconstructed Au(110) Surfaces. *Surf. Sci.* **1983**, *131* (1), 379–384.
(78) Moritz, W.; Wolf, D. Multilayer Distortion in the Reconstructed (110) Surface of Au. *Surf. Sci.* **1985**, *163* (1), 655–665.
(79) Hiebel, F.; Montemore, M. M.; Kaxiras, E.; Friend, C. M. Direct Visualization of Quasi-Ordered Oxygen Chain Structures on Au(110)-(1 × 2). *Surf. Sci.* **2016**, *650*, 5–10.
(80) Xu, F.; Madix, R. J.; Friend, C. M. Spatially Nonuniform Reaction Rates during Selective Oxidation on Gold. *J. Am. Chem. Soc.* **2018**, *140* (38), 12210–12215.
(81) Landmann, M.; Rauls, E.; Schmidt, W. G. Chainlike Au–O Structures on Au(110)-(1 × r) Surfaces Calculated from First Principles. *J. Phys. Chem. C* **2009**, *113* (14), 5690–5699.
(82) Tersoff, J.; Hamann, D. R. Theory of the Scanning Tunneling

Microscope. *Phys. Rev. B* **1985**, *31* (2), 805–813.
(83) Maksymovych, P.; Mezhenny, S.; Yates, J. T. STM Study of Water Adsorption on the TiO_2(110)-(1 × 2) Surface. *Chem. Phys. Lett.* **2003**, *382* (3–4), 270–276.
(84) Diebold, U. Structure and Properties of TiO_2 Surfaces: A Brief Review. *Appl. Phys. A* **2003**, *76*, 681–687.
(85) Zhou, C.; Ren, Z.; Tan, S.; Ma, Z.; Mao, X.; Dai, D.; Fan, H.; Yang, X.; Larue, J.; Cooper, R.; Wodtke, A. M.; Wang, Z.; Li, Z.; Wang, B.; Yang, J.; Hou, J. Site-Specific Photocatalytic Splitting of Methanol on TiO_2(110). *Chem. Sci.* **2010**, *1* (5), 575–580.
(86) Hammer, B.; Wendt, S.; Besenbacher, F. Water Adsorption on TiO_2. *Top. Catal.* **2010**, *53*, 423–430.
(87) Lee, J.; Sorescu, D. C.; Deng, X.; Jordan, K. D. Water Chain Formation on TiO_2(110). *J. Phys. Chem. Lett.* **2013**, *4* (1), 53–57.
(88) Setvin, M.; Daniel, B.; Aschauer, U.; Hou, W.; Li, Y. F.; Schmid, M.; Selloni, A.; Diebold, U. Identification of Adsorbed Molecules via STM Tip Manipulation: CO, H_2O, and O_2 on TiO_2 Anatase (101). *Phys. Chem. Chem. Phys.* **2014**, *16* (39), 21524–21530.
(89) Dette, C.; Pérez-Osorio, M. A.; Mangel, S.; Giustino, F.; Jung, S. J.; Kern, K. Atomic Structure of Water Monolayer on Anatase TiO_2 (101) Surface. *J. Phys. Chem. C* **2018**, *122* (22), 11954–11960.
(90) Wendt, S.; Schaub, R.; Matthiesen, J.; Vestergaard, E. K.; Wahlström, E.; Rasmussen, M. D.; Thostrup, P.; Molina, L. M.; Lægsgaard, E.; Stensgaard, I.; Hammer, B.; Besenbacher, F. Oxygen Vacancies on TiO_2(110) and their Interaction with H_2O and O_2: A Combined High-Resolution STM and DFT Study. *Surf. Sci.* **2005**, *598* (1–3), 226–245.
(91) Di Valentin, C.; Tilocca, A.; Selloni, A.; Beck, T. J.; Klust, A.; Batzill, M.; Losovyj, Y.; Diebold, U. Adsorption of Water on Reconstructed Rutile TiO_2(011)- (2×1): Ti=O Double Bonds and Surface Reactivity. *J. Am. Chem. Soc.* **2005**, *127* (27), 9895–9903.
(92) Allegretti, F.; O'Brien, S.; Polcik, M.; Sayago, D. I.; Woodruff, D. P. Adsorption Bond Length for H_2O on TiO_2(110): A Key Parameter for Theoretical Understanding. *Phys. Rev. Lett.* **2005**, *95* (22), 226104.
(93) Bikondoa, O.; Pang, C. L.; Ithnin, R.; Muryn, C. A.; Onishi, H.; Thornton, G. Direct Visualization of Defect-Mediated Dissociation of Water on TiO_2(110). *Nat. Mater.* **2006**, *5*, 189–192.
(94) Pang, C. L.; Sasahara, A.; Onishi, H.; Chen, Q.; Thornton, G. Noncontact Atomic Force Microscopy Imaging of Water Dissociation Products on TiO_2. *Phys. Rev. B* **2006**, *74* (7), 073411.
(95) Teobaldi, G.; Hofer, W. A.; Bikondoa, O.; Pang, C. L.; Cabailh, G.; Thornton, G. Modelling STM Images of TiO_2(110) from First-Principles: Defects, Water Adsorption and Dissociation Products. *Chem. Phys. Lett.* **2007**, *437* (1–3), 73–78.
(96) Cui, X.; Wang, Z.; Tan, S.; Wang, B.; Yang, J.; Hou, J. G. Identifying Hydroxyls on the TiO_2(110)-1 × 1 Surface with Scanning Tunneling Microscopy. *J. Phys. Chem. C* **2009**, *113* (30), 13204–13208.
(97) Matthiesen, J.; Wendt, S.; Hansen, J.; Madsen, G. K. H.; Lira, E.; Galliker, P.; Vestergaard, E. K.; Schaub, R.; Lægsgaard, E.; Hammer, B.; Besenbacher, F. Observation of All the Intermediate Steps of a Chemical Reaction on an Oxide Surface by Scanning Tunneling Microscopy. *ACS Nano* **2009**, *3* (3), 517–526.
(98) Dementyev, P.; Dostert, K.; Ivars-Barceló, F.; O'Brien, C. P.; Mirabella, F.; Schauermann, S.; Li, X.; Paier, J.; Sauer, J.; Freund, H. Water Interaction with Iron Oxides. *Angew. Chemie Int. Ed.* **2015**, *54* (47), 13942–13946.
(99) Meier, M.; Hulva, J.; Jakub, Z.; Pavelec, J.; Setvin, M.; Bliem, R.; Schmid, M.; Diebold, U.; Franchini, C.; Parkinson, G. S. Water Agglomerates on Fe_3O_4(001). *Proc. Natl. Acad. Sci. U. S. A.* **2018**, *115* (25), E5642–E5650.
(100) Xu, B.; Haubrich, J.; Baker, T. A.; Kaxiras, E.; Friend, C. M. Theoretical Study of O-Assisted Selective Coupling of Methanol on Au(111). *J. Phys. Chem. C* **2011**, *115* (9), 3703–3708.
(101) Sicinska, D.; Truhlar, D. G.; Paneth, P. Solvent-Dependent Transition States for Decarboxylations. *J. Am. Chem. Soc.* **2001**, *123* (31), 7683–7686.
(102) Mellmer, M. A.; Sener, C.; Gallo, J. M. R.; Luterbacher, J. S.; Alonso, D. M.; Dumesic, J. A. Solvent Effects in Acid-Catalyzed Biomass Conversion Reactions. *Angew. Chemie - Int. Ed.* **2014**, *53* (44), 11872–11875.
(103) Mellmer, M. A.; Sanpitakseree, C.; Demir, B.; Bai, P.; Ma, K.; Neurock, M.; Dumesic, J. A. Solvent-Enabled Control of Reactivity for Liquid-Phase Reactions of Biomass-Derived Compounds. *Nat. Catal.* **2018**, *1*, 199–207.
(104) Eagan, N. M.; Luneau, M.; Friend, C. M.; Madix, R. J. Exploiting the Liquid Phase to Enhance the Cross-Coupling of Alcohols over Nanoporous Gold Catalysts. *ACS Catal.* **2022**, *12* (1), 183–192.
(105) Magnussen, O. M.; Groß, A. Toward an Atomic-Scale Understanding of Electrochemical Interface Structure and Dynamics. *J. Am. Chem. Soc.* **2019**, *141* (12), 4777–4790.
(106) Nørskov, J. K.; Rossmeisl, J.; Logadottir, A.; Lindqvist, L.; Kitchin, J. R.; Bligaard, T.; Jónsson, H. Origin of the Overpotential for Oxygen Reduction at a Fuel-Cell Cathode. *J. Phys. Chem. B* **2004**, *108* (46), 17886–17892.
(107) Casalongue, H. S.; Kaya, S.; Viswanathan, V.; Miller, D. J.; Friebel, D.; Hansen, H. A.; Nørskov, J. K.; Nilsson, A.; Ogasawara, H. Direct Observation of the Oxygenated Species during Oxygen Reduction on a Platinum Fuel Cell Cathode. *Nat. Commun.* **2013**, *4*, 2817.
(108) Ledezma-Yanez, I.; Wallace, W. D. Z.; Sebastián-Pascual, P.; Climent, V.; Feliu, J. M.; Koper, M. T. M. Interfacial Water Reorganization as a pH-Dependent Descriptor of the Hydrogen Evolution Rate on Platinum Electrodes. *Nat. Energy* **2017**, *2*, 17031.
(109) Velasco-Velez, J.-J.; Wu, C. H.; Pascal, T. A.; Wan, L. F.; Guo, J.; Prendergast, D.; Salmeron, M. The Structure of Interfacial Water on Gold Electrodes Studied by X-Ray Absorption Spectroscopy. *Science* **2014**, *346* (6211), 831–834.
(110) Li, C. Y.; Le, J. B.; Wang, Y. H.; Chen, S.; Yang, Z. L.; Li, J. F.; Cheng, J.; Tian, Z. Q. In Situ Probing Electrified Interfacial Water Structures at Atomically Flat Surfaces. *Nat. Mater.* **2019**, *18*, 697–701.
(111) Wu, C. H.; Pascal, T. A.; Baskin, A.; Wang, H.; Fang, H. T.; Liu, Y. S.; Lu, Y. H.; Guo, J.; Prendergast, D.; Salmeron, M. B. Molecular-Scale Structure of Electrode-Electrolyte Interfaces: The Case of Platinum in Aqueous Sulfuric Acid. *J. Am. Chem. Soc.* **2018**, *140* (47), 16237–16244.
(112) Benziger, J. B.; Ko, E. I.; Madix, R. J. The Decomposition of Formic Acid on W(100) and W(100)-(5×1) C Surfaces. *J. Catal.* **1979**, *58* (1), 149–153.

For Table of Contents Only